Kyere *et al. Int. J. Air-Cond. Ref.* (2023) 31:28
https://doi.org/10.1007/s44189-023-00045-5

International Journal of
Air-Conditioning and Refrigeration

RESEARCH Open Access

Parametric analysis of chiller plant energy consumption in a tropical climate

Esther Benedicta Kyere[1], Jen Tien-Chien[1] and Lagouge Tartibu[2*]

Abstract

The approach that could reduce the energy consumption of water-cooled chillers in office buildings was investigated through experimental and simulation methods. The chiller was modelled in TRNSYS and validated using physical measurements from an operational water-cooled water chiller and fan coil system. The validated model was used to analyse the energy consumption of the water chiller-fan coil system under a high chilled water temperature setpoint (CWTS) in a representative commercial office building. Subsequently, indoor thermal comfort was evaluated using the PMV-PPD model. Finally, the design of experiment (DOE) was employed using a statistical two-level non-randomized factorial design in Minitab to study the effects of high CWTS, number of rows, and tube diameter on the heat and mass transfer performance of the fan coil unit. The results showed that the CWTS can be increased by various degrees from 10 up to 18 °C for energy efficiency for a commercial office building in the tropics. This increase in CWTS would result in a daily energy saving potential of about 5% of the chiller as compared to the existing operational settings without any extra cost. Conversely, the daily energy consumption by the fan coil would increase by about 5.5% by this increment in the CWTS. It was determined that the chiller system can provide comfort even when the CWTS is increased to 14 °C. The DOE analysis showed that under the condition of high CWTS (14 °C), energy consumption that is less than the current energy consumption may be expected from the fan coil system when the number of rows increased from 3 to 6 and the tube diameter increased from 7 to 9 mm.

Keywords Chilled water temperature setpoint, Fan coil system, Energy saving, PMV-PPD, DOE, TRNSYS simulation

1 Introduction

In a tropical climate, there is the challenge of maintaining comfortable indoor thermal conditions in a building space. This arises due to the persistent discomfort within the building area caused by elevated temperatures, high relative humidity, and insufficient air circulation [1]. These factors collectively contribute to a state of thermal discomfort within indoor environments. Chilled water plants are commonly used to provide cooling in these spaces. However, the chiller plant operation is not optimal in most of the existing buildings because the chiller plant is either operated at design conditions irrespective of the cooling load or optimized locally due to a lack of overall chiller plant behaviour. People living in hot and humid countries tend to use the air conditioner (AC) by setting it at the lowest set point temperature [2]. Likewise, the chiller system, the lowest chilled water temperature setpoint (CWTS) is usually selected for indoor thermal comfort. However, such low-temperature settings consume more energy [3] and harm the environment by producing indirect emissions due to their high energy consumption [4]. To deal with this, it is critical to optimize the amount of energy consumed by the chiller systems in buildings as well as to attain good indoor environment conditions. People nowadays spend a considerable portion of their time (60–90%) inside buildings [5]

*Correspondence:
Lagouge Tartibu
ltartibu@uj.ac.za
[1] Mechanical Engineering Science, University of Johannesburg, Johannesburg, South Africa
[2] Mechanical and Industrial Engineering Technology, University of Johannesburg, Johannesburg, South Africa

probably due to the harsh environmental conditions as a result of climate change or the COVID-19 pandemic. As a result, the quality of occupied spaces is an important consideration for maintaining a healthy indoor environment [6]. Chillers, cooling towers, pumps, and chilled water storage tanks are typical components of a chiller plant [7] frequently utilized to cool large office buildings or multi-building campuses [8] for indoor thermal comfort of occupants [6] and their efficiency [9]. Notwithstanding, the chiller system consumes more than 40% of the total electricity used in a building [10]. Consequently, effective energy management of chiller plants is becoming increasingly necessary to reduce energy consumption and environmental consequences [11]. There has been a lot of study and research in the literature for optimizing one of the components of a chiller plant [12–14] for energy efficiency. Lu and Cai [15] developed mathematical models that linked cooling loads and energy consumption to create optimal setpoints established on sensor data. It was discovered that operating the chilled water system at optimal chilled water supply temperature, chilled water pump head, and other setpoints resulted in significant energy savings. Chan and Yu used a simulation tool to create a chiller model [16]. The optimal condensing water temperature set point for chillers was discovered and regulated, resulting in less variation in chiller efficiency under various operating situations. But the interactions between components are ignored for those improvements focusing on optimizing a single component of a chiller plant. A chiller system, in reality, is a system in which components influence and are influenced by the plant's functioning. Several factors, in addition to the components themselves, affect the energy consumption of a chiller plant. Weather conditions, the quantity and nature of operational hours, facility usage, and cooling demands are among the factors that should be taken into account [17]. While considering these factors to manage a chiller plant to optimize energy efficiency, it is necessary to analyse the relationships and factors [7]. Design of experiment (DOE) is a systematic, efficient method that enables scientists and engineers to study the relationship between multiple input variables and key output variables. It is therefore very good and effective in multi-factor study of the combined effects of the factors on the design of a commodity under study. It is also used to reduce the cost of conducting several physical experiments. The energy consumption of a heat source was reduced by raising the chilled water temperature higher than 7 °C in the fan-coil AC system [18]. Also, when the chiller supply temperature was increased from 7 to 9 °C and the chilled water temperature difference was adjusted from 5 to 9 °C. Ha et al. [19] showed through EnergyPlus modelling that the energy of the cooling system of a large office building can be lowered by 6%. However, a high CWTS may lead to reduced cooling and dehumidifying capacity of the fan coil. Thus, the effects of high CWTS on the heat and mass transfer performance of the fan-coil should be analysed as indoor thermal comfort is critical to consider when optimizing the energy efficiency of the chiller plant. The management of energy efficiency and thermal comfort is a major concern for building designers and managers [20, 21]. Previously, concerns relating to Indoor Air Quality (IAQ) were treated independently from those relating to building energy efficiency [22]. As a result, many case studies in the literature only look at one part. However, instances of a combined strategy are shown, such as the work of Mancini *et al.* [23], building energy consumption and Indoor Environmental Quality (IEQ) were evaluated by varying the airflow rates handled by the HVAC system. Equally, efforts were made to reduce energy consumption in school buildings while also ensuring sufficient indoor environmental conditions, as conducted by Karami *et al.* [24]. Vilčeková et al. [25] conducted an evaluation of Indoor Air Quality (IAQ) in residential buildings, involving the assessment of environmental parameters such as temperature, relative humidity, and concentrations of significant contaminants. A measurement technique for tracking the performance of a building was presented in the work of Mancini *et al.* [23]. The study concentrated on Indoor Environmental Quality; sensors were used for detecting air temperature, relative humidity, illuminance, and occupancy in the system. However, in this COVID-19 era, it is vital to consider occupant health when optimizing the energy consumption of a chiller system. Given this, the predicted mean vote (PMV) model by Fanger [26] is the most extensively used index. The PMV index was developed based on an analysis of the human body's heat balance taking into account physical environment variables such as air temperature, air velocity, clothing insulation level, metabolic rate, and relative humidity [27]. The International Standards Organization (ISO) 7730 [28] and the American Society of Heating, Refrigerating, and Air Conditioning Engineers (ASHRAE) Standard 55 [29] respectively accept PMV index ranges of 0.5 to +0.5 and 0.7 to +0.7 for thermal comfort. The predicted percentage dissatisfied (PPD) values are $\leq$ 10% and $\leq$ 15% based on ASHRAE and ISO, respectively, and their corresponding allowable PMV index limits. Several studies have used the PMV model to predict the impact of thermal comfort on building energy consumption. The thermal comfort and energy consumption in a residential building using the PMV control and considering the metabolic rate of each occupant were evaluated by Hong et al. [30]. The above literature review reveals that a lot of studies have been conducted in the area of managing the

chiller system for energy efficiency and indoor thermal comfort. However, not much has been done to investigate the effect on individual components of the chiller system during the managing process. This study aimed to investigate the performance of the main chiller system components under varied CWTS through experiments and numerical simulations and to study the performance of the fan coil unit under high CWTS. The novelty of this study is the use of mixed methods, TRNSYS, and DOE selection criteria to identify particular optimization approaches that satisfy the current design and functional constraints of the chiller system. The significance of this research is to better understand the performance and design optimization of the chiller system with high CWTS in the air conditioning system and to provide guidance for future design advancements. To achieve this, experiments are conducted in a chiller-fan coil system where the CWTS is varied from 10 to 14 °C. The influence of the various CWTS on the performance of the chiller system is experimentally determined by measuring the power consumption of the chilled water cycle components (chiller, pump, and fan coil unit), indoor temperature, and relative humidity. Simulation of the chiller system is performed in TRNSYS to predict the energy consumption of the various components beyond the CWTS range. In addition, DOE is used to study how the fan coil unit could be improved by varying influential parameters (inside tube diameter, number of rows, and CWTS) on air temperature, logarithmic mean temperature difference (LMTD), and heat transfer coefficient (HTC).

2 Materials and methods

2.1 Description of the experimental site

The analysed case study is the Takoradi Thermal Power Plant office building situated at Takoradi, Ghana (4.9716° N, 1.6586° W), which can be considered a relevant example of a commercial office building. The experimental site is in a tropical savannah climate with an annual average temperature of 26.1 °C. On average, the warmest month is March, boasting an average temperature of 27.3 °C, while the coolest month is August. The average annual precipitation for the year in Takoradi is 1292.9 mm. The highest monthly precipitation on average is June with 332.7 mm of precipitation, and the least precipitation on average is January with an average of 25.4 mm.

2.2 Experimental setup

The chilled water system (water-cooled chilled water system) consists of three hydronic cycles, namely: (a) primary condensing cycle that consists of three submersible pumps circulating seawater to the three heat exchangers and a sump (b) secondary condensing cycle that consists of twin head pumps circulating fresh water to the condensers in the chillers then to the heat exchangers (c) the chilled water cycle consisting of the chiller and pumps that circulate chilled water to the fan coils. The chilled water cycle was used for the analysis. It comprises a water-cooled water chiller with a cooling capacity of 240 kW, a 25 kW MFCL-30-030573 fan coil unit model, (with direct-drive, forward-curved blower) that produces 1.89 m^3/s supply air of dimensions of 1550 mm × 620 mm ×520 mm, a condenser water pump of 16 kW capacity and a 9.2 kW capacity chilled water centrifugal pump. The chilled water cycle (chiller, pump, and fan coil units) which serves the experimental room (drivers' office) consists of a water-cooled water chiller that serves nine fan coil units, a pump serving nine fan coil units, and each fan coil unit serving two or three dedicated rooms in the office complex. The chilled water cycle is coupled to a seawater reservoir for heat exchange. The experiment was limited to one room (the drivers' office—5100 mm × 3560 mm × 2743.2 mm) due to availability. The chiller serving the experimental room (drivers' room) runs for 9 h and 20 min daily. The cooling load for the chiller system typically comprises four main components: the transmission load, infiltration load, solar load, and internal load. Transmission load refers to the heat gain resulting from a temperature disparity across building elements like walls and window frames. The infiltration load results from the entry of outdoor air into a conditioned area through openings like doors and windows. leading to heat gain. Solar load arises from the heat gain caused by direct solar radiation transmission. The amount of radiation that enters the building directly is established by the solar transmittance of the windows. The internal load represents the sensible heat load resulting from the emission of heat within a space, which can be attributed to sources like lighting, equipment, and occupants. The driver's office has a table, chairs, lights, and a cabinet with an occupancy of six people at any point in time. The drivers' office has two diffusers of dimension 650 mm × 440 mm positioned at 1300 mm away from each opposite wall. The ceiling material was constructed of gypsum tiles, the roofing was made of concrete material, and the room was fitted with a galvanized moulded door. The lighting, occupancy, and related components in the driver's room produce heat and constitute the cooling load of the space. The schematic diagram of the chilled water cycle and the experimental setup are shown in Figs. 1 and 2. The equipment used to measure experimental data included an energy meter, temperature, and humidity sensors. Indoor air temperature, relative humidity, and outdoor temperature and relative humidity were measured. Hobo

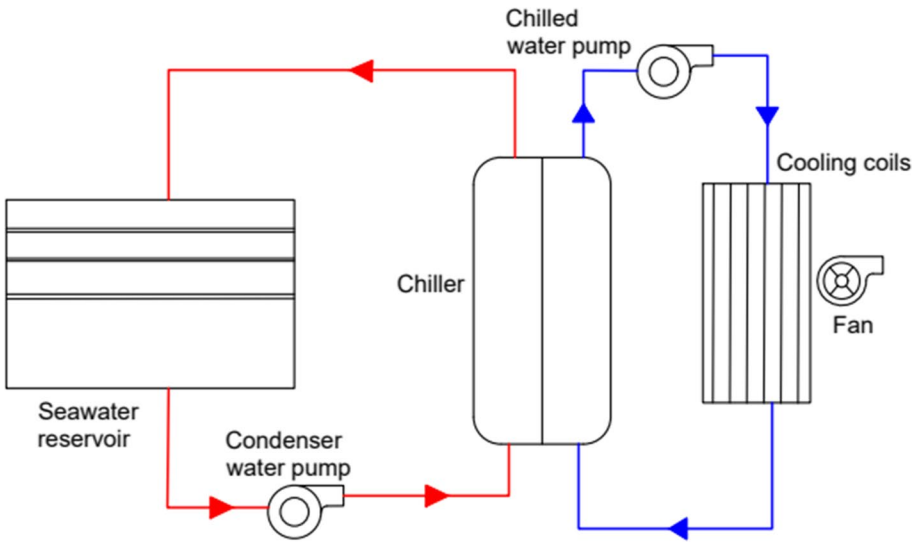

Fig. 1 Schematic diagram of the chiller system used for the study

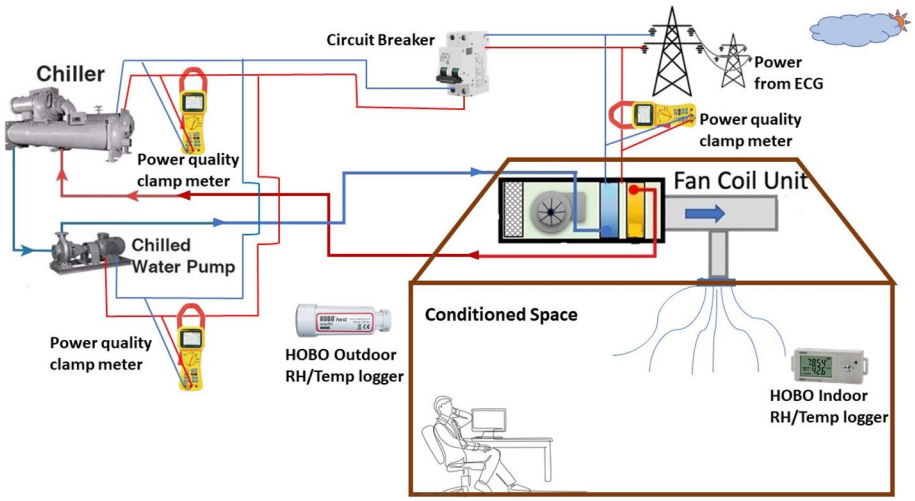

Fig. 2 Experimental setup

temperature and relative humidity data loggers were used to measure the air temperature and relative humidity.

The hobo device measuring indoor temperature had a range of −20 to 70 °C and an accuracy of ± 0.21 °C from −20 to 70 °C. The hobo device measuring indoor relative humidity had a range of 1 to 90% and an accuracy of ± 2.5% from 1 to 90%. The Hobo U23 Pro v2 temp. data logger for measuring the outdoor temperature and relative humidity had a range of −40 to 70 °C and 0 to 100% RH and accuracy of ± 0.25 °C from −40 to 70 °C and ± 2.5% from 0 to 100% RH, respectively. The Fluke-345 Power meter used to measure the energy consumption had a rating of Max 40,000 kWHr and an accuracy of 2 kWHr, ± 3% ± 5 digits.

2.3 Precision of experimental data

The standard error (SE) is a statistical measure that quantifies the variability or uncertainty associated with a sample statistic, typically the sample mean. It is a way to estimate how much the sample mean is likely to vary from the true population mean. A smaller SE indicates that the sample mean is a more reliable estimate of the population mean. On the other hand, a larger SE suggests a greater degree of variability in the data. The assessment of experimental uncertainty was conducted using the

standard error of the mean, a statistical approach that encompasses repeatability and reproducibility experiments. The experiments were conducted at three different chilled water temperature setpoints: 10 °C, 12.5 °C, and 14 °C. Uncertainty was determined from the analysis of the three experiments using the formula in Eq. 1. The SE of the energy consumption at 10 °C, 12.5 °C, and 14 °C CWTS is 0.32 kWh, 0.17 kWh, and 0.36 kWh, respectively. Thus, the results indicate a mean energy consumption of 87.84 ± 0.32 kWh, 86.83 ± 0.17 kWh, and 85.57 ± 0.36 kWh for 10 °C, 12.5 °C, and 14 °C CWTS. The SE values suggest that the precision of this experimental data is reliable for use in further experimental analysis

$$\text{Standard Error} = \frac{\text{Standard Deviation } (\sigma)}{\sqrt{(\text{Sample Sise})}} \quad (1)$$

2.4 Data collection and analysis

Data was logged in terms of the following parameters: indoor temperature, relative humidity, power consumption, outdoor relative humidity, and outdoor temperature. In this study, sensors were placed at an average height of 1.1 m for sitting occupants' configuration and 1.7 m for standing occupant configuration [27]. Indoor measurements were taken in one of the building's offices (the driver's room), and outdoor measurements were taken near the office's entrance. At each chilled water temperature setpoint (10 °C, 12.5 °C, and 14 °C), data from the chiller system and the indoor environment parameters were recorded. The experiment was carried out during an occupancy period, from 7:00 a.m. to 4:20 p.m., Monday to Friday, from June 30 to July 10, 2020. The experiment was conducted on 3 consecutive days, for each chilled water temperature setpoint. Indoor environment parameters (air temperature and relative humidity) of the room and power consumed by the chiller components were recorded within 1 min intervals continuously throughout the experimental period.

Data analysis was conducted using mixed approaches which involved using mathematical modelling (TRNSYS simulation used to examine the building's energy performance), predicted mean vote (PMV), and predicted percentage dissatisfied (PPD), (used to analyse the thermal comfort conditions in the experimental room) and design of experiment (DOE) used to analyse the effect of primary factors on air temperature, logarithmic mean temperature difference (LMTD) and heat transfer coefficient of the fan coil. The indoor thermal conditions considered in this study were temperature and relative humidity measurements. The measured average temperature and relative humidity parameters were then used as input to the ASHRAE Thermal Comfort tool.

2.5 Mathematical modelling and simulation

The building energy systems software used to model the chiller system was TRNSYS 17. TRNSYS is a transient system simulation software with a modular structure that was created to handle complicated energy systems by breaking them down into smaller components [31]. In TRNSYS, these components are referred to as "Types". TRNSYS Simulation Studio, which is a complete combined visual interface, is used to configure and assemble the Types (components). TRNSYS includes a simulation solver that can solve both algebraic and differential equations. The components that constitute the chiller system (chiller, fan coil unit, pump, reservoir, and reference room) were selected, specified, and connected according to the field setup. The TRNSYS 17 mathematical component and references were used as a guide in selecting the most appropriate components for creating the chiller system [32]. The component information was taken from the manufacturer's specification sheets.

2.5.1 Boundary conditions setup

Presented in Fig. 3 is the schematic of the chiller system model built in TRNSYS. The Type 88 component which is the lumped capacitance building component with internal gains was used to model the drivers' office. This component neglects the solar gains and assumes an overall heat transfer coefficient (U) value for the entire room. The Type 88 component was chosen due to its usefulness which is attributable to the speed with which a building cooling and heating load can be added to a system's simulation. The Chiller Type 107 was selected together with the fan coil unit components (Type 92 (Auxiliary cooling unit), Type 112b (Fan), Type 32 (cooling coil) and Type 3d (pump), Type 4a (a stratified storage tank), Type 8a (a five-stage room thermostat). The TRNSYS model was developed using a progressive incorporation strategy. This strategy involved the initial creation, adjustment, and validation of the building model with the experimental data. The various components of the chiller system were added to the TRNSYS model progressively (the fan coil unit followed by the chiller, stratified tank, the five-stage thermostat, and the pumps). The daily building operation schedule of the drivers' office was from 7:00 a.m. to 4:20 p.m. (Monday to Friday). The cooling control system was set to the chilled water temperature setpoint (CWTS) ranging from 10 to 14 °C depending on the season of the year, occupancy, and prevailing ambient conditions. The energy consumption for lighting used was estimated at 17 W/m^2. The office uses fluorescent lights to supplement the natural lighting which is inadequate due to the use of window blinds. The meteorological (climatic) data in the form of a Typical Meteorological

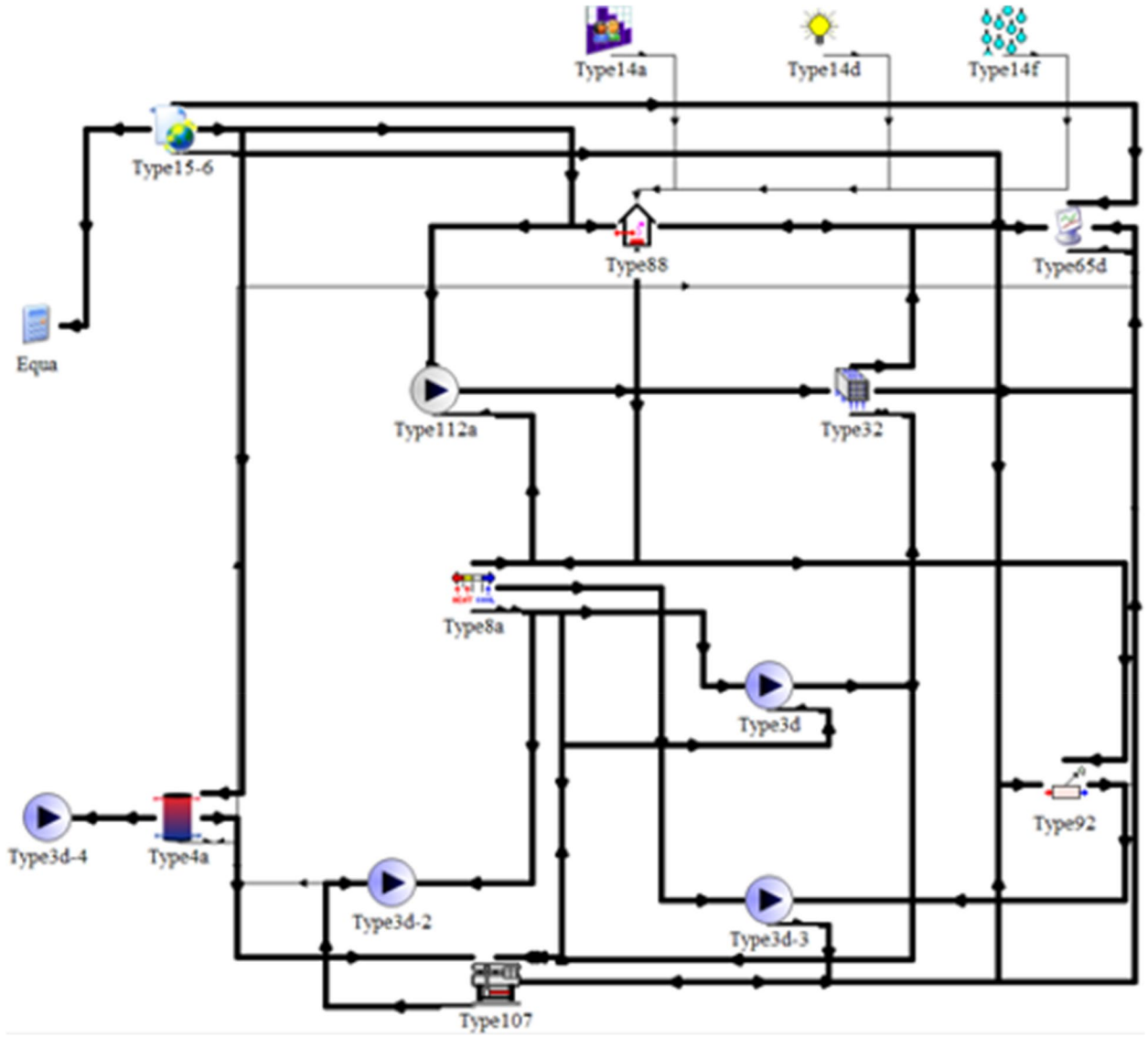

Fig. 3 Schematic of the chiller system model built in TRNSYS

Year (TMY) for the city of Takoradi was used. This TMY file is built into the TRNSYS Weather Data Reading and Processing System. The input weather file is based on the ground weather station and satellite data. Minutes and hourly values of the dry bulb temperature, relative humidity, wind direction, speed, and direct solar horizontal radiation were used in the simulation.

Three alternative operating conditions were simulated in TRNSYS, as indicated in Table 3, specifically: usual operation (Default CWTS at 12.5 °C) scenario #1,

Table 1 Specifics of the scenario under consideration

Scenario	Relative CWTS	Parameters analysed	
		Simulation	Measurement taken
Scenario # 1	12.5 °C	Energy consumption	Energy consumption, temperature, relative humidity, PMV, and PPD
Scenario # 2	10 °C	Energy consumption	Energy consumption, temperature, relative humidity PMV, and PPD
Scenario # 3	14 °C	Energy consumption	Energy consumption, temperature, relative humidity, PMV, and PPD

as well as two more scenarios including the increase and decrease of the chiller plant's CWTS to 14 °C (scenario #2) and 10 °C (scenario #3). The details of each scenario are summarized in Table 1.

2.5.2 Model validation

The developed mathematical model (TRNSYS) was validated by comparing the mathematical model results against the experimentally measured values using some error validation models. These error validation models enable the researcher to determine the accuracy of the developed mathematical model. The error validation models employed in this study are the percentage bias (PBIAS), mean absolute error (MAE), root mean squared error (RMSE), and mean square error (MSE). The equations for the aforementioned validation models are presented in Eqs. (2) to (4) [33, 34]. The percentage bias (PBIAS) quantifies the average tendency of the predicted value to be greater or smaller than their measured counterparts [35]. The ideal value of PBIAS is 0.0, and low magnitude values represent an accurate model simulation. Underestimation bias is indicated by positive values, whereas overestimation bias is indicated by negative values [34]. The RMSE-observations standard deviation ratio (RSR) is calculated as the ratio of the RMSE and the standard deviation of measured data. RSR varies from the optimal value of 0 to a large positive value. The lower the RSR, the lower the RMSE, and the better the model simulation performance. When the RMSE is equal to zero, the measured and predicted values match perfectly, and as the RMSE increases, the match gets worse. According to Karunasingha [36], RMSE values that are less than half the standard deviation of the measured data may be regarded as low and suggestive of a good model prediction.

$$PBIAS = \left[\frac{\sum_{i=1}^{n}\left(y_i - \hat{y}_i\right) \times (100)}{\sum_{i=1}^{n}\left(y_i\right)}\right] \tag{2}$$

where y_i is the ith observed value, and $\hat{y}_i$ is the corresponding predicted value.

$$MAE = \frac{\sum_{i=1}^{n}\left|\left(y_i - \hat{y}_i\right)^2\right|}{n} \tag{3}$$

where y_i is the ith observed value, $\hat{y}_i$ is the corresponding predicted value, and n is the number of observations.

Table 2 Design summary for the experiments

Design summary			
Factors	3	Replicates	1
Base Runs	8	Total runs	8
Base Blocks	1	Total blocks	1

Table 3 Factor information

Factor	Levels	Values
Tube diameter	2	7, 9
Number of rows	2	3, 6
CWTS	2	10, 14

$$RSR = \frac{RMSE}{STDEV_{obs}} = \frac{\left[\sqrt{\sum_{i=1}^{n}\left(y_i - \hat{y}_i\right)^2}\right]}{\left[\sqrt{\sum_{i=1}^{n}\left(y_i - y^{\text{mean}}\right)^2}\right]} \tag{4}$$

where y_i is the ith observed value, $\hat{y}_i$ is the corresponding predicted value, and y^{mean} is the mean of observations.

$$RMSE = \sqrt{\sum_{i=1}^{n}\frac{\left(y_i - \hat{y}_i\right)^2}{n}} \tag{5}$$

where y_i is the ith observed value, $\hat{y}_i$ is the corresponding predicted value, and n is the number of observations.

2.6 Design of experiment (DOE)

The ability of the fan-coil to transport heat and mass is highly influenced by the configuration of the coil (rows, diameter, tube spacing, etc.) and flow temperature. To guarantee the cooling and dehumidification capability of a fan coil with high CWTS, the method of increasing the heat transfer area, for example adding the number of rows, tube diameter, and tube spacing, is more economical and practical [37]. Therefore, using the design of experiments (DOE), a two-level non-randomized factorial experimental design with no replication was planned. Three main factors (inside tube diameter (mm), the number of rows, and CWTS (°C)) that affect the thermal behaviour of the fan coil were taken into account when conducting the experiments. Three rows of fan-coil were selected since it is the specification that is typically used in the standard air conditioning system [37]. Additionally, the maximum number of rows for fan-coil specifications led to the selection of six rows for the fan-coil [38]. The experiments had a total of eight runs. The design summary for the experiments and the factor information

Table 4 Experimental matrix for effects of inside tube diameter, number of rows, and CWTS on supply temperature, LMTD, heat transfer coefficient

Level values	Factor			Response		
	Tube diameter (mm)	Number of rows	CWTS (°C)	Air temperature (°C)	LMTD (°C)	Heat transfer coefficient ($W/m^2 \cdot K$)
1	7	3	10	23.29	6.63	306.59
2	7	3	14	24.93	5.09	308.28
3	7	6	10	23.26	6.64	285.99
4	7	6	14	24.18	5.11	295.24
5	9	3	10	23.31	6.64	306.60
6	9	3	14	24.93	5.32	308.30
7	9	6	10	23.20	6.62	285.90
8	9	6	14	24.16	5.10	287.2

are shown in Tables 2 and 3, respectively. To analyse the heat and mass transfer of the fan coil, the effect of the main factors on air temperature, the LMTD, and the heat transfer coefficient was analysed. Table 4 shows the experimental matrix for the effects of inside tube diameter, number of rows, and CWTS on air temperature, LMTD, and heat transfer coefficient. The variables: inner tube diameter, number of rows, and CWTS each had two level values in all the three experiments. The DOE was carried out using Minitab statistical software, version 19.

3 Results and discussion

3.1 Simulation of thermal comfort indices PMV-PPD in the experimental room

Indoor environmental health is essential in chiller design. The occupants in an enclosed environment (in this case indoor room) could suffer from discomfort and serious health complications if the indoor environment is not well managed. Occupants in an indoor environment may be exposed to the following: temperature variations, relative humidity variations, carbon dioxide concentration, particulate matter, bacteria, viruses (e.g., coronavirus) [39] as well as other gases (carbon monoxide, hydrogen sulphide, ammonia) [40]. Using the ASHRAE comfort tool, the thermal comfort indices (PMV and PPD) were simulated for 9 h, 20 min a day, from 7:00 to 16:20, for CWTS 10 °C, 12.5 °C, and 14 °C. The mean temperature and relative humidity were used as inputs to the tool. The metabolic activity of 1.0 met, air velocity of 0.1 m/s, and the clothes thermal resistance of 0.6 Clo from literature which corresponds to the conditions in the room were used. Figs. 4a and b present the plot of indoor air temperature and relative humidity against the time of operation and the corresponding PMV and PPD at each

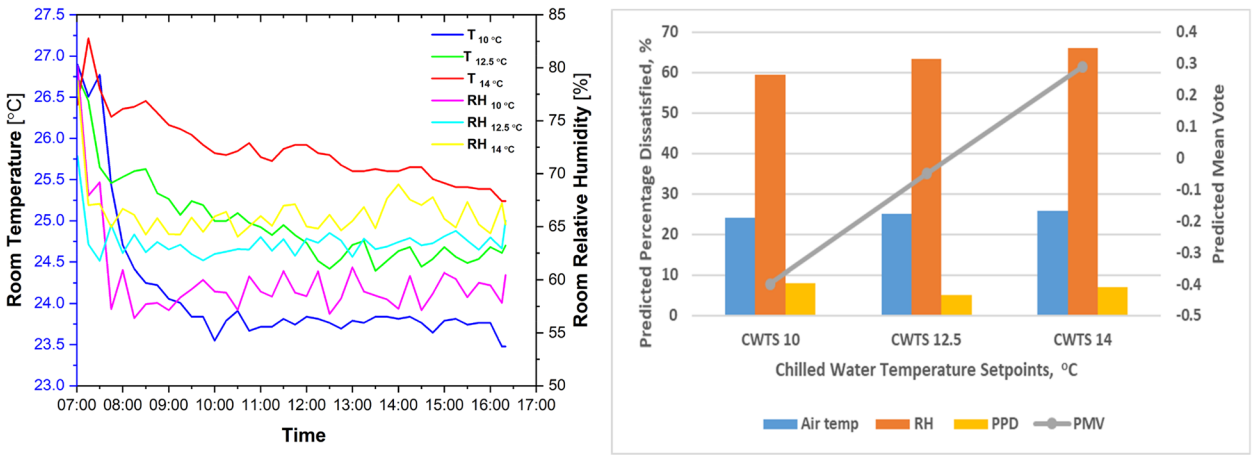

(a) (b)

Fig. 4 **a** Indoor temp. and RH against time. **b** CWTS against PPD and PMV

CWTS, respectively. According to ISO 7730, an acceptable indoor climate is when PMV is in the range of ± 0.5 and PPD is below 10% [28]. From Fig. 4a, all the CWTS had their mean indoor air temperatures ranging from 23 to 26.8 °C. While indoor relative humidity readings were slightly elevated, ranging from 59 to 67%, this may not be a significant concern due to the occupants' adaptive capabilities [41]. Consequently, indoor relative humidity levels up to 70% are unlikely to adversely impact thermal comfort [42]. Hence, the assessment of the office space solely based on measured temperatures would rate the room as being comfortable or uncomfortable [43]. That notwithstanding, the high relative humidity levels could be a result of the high CWTS. Based on the concept of heat exchange, the high CWTS could cause a reduction in the cooling and dehumidifying capacity of the fan coil as demonstrated in Fig. 4a because of the small logarithmic mean temperature difference (LMTD) between the indoor air and the chilled water in the fan-coil. The simulation results shown in Fig. 4b demonstrate the effect of CWTS on PMV and PPD. Resetting the CWTS led to variations in PMV and PPD. However, resetting the CWTS from 10 to 14 °C and holding other variables (metabolic activity of 1.0 met, the air velocity of 0.1 m/s, and the clothes thermal resistance of 0.6 Clo) constant cause an increase in the PMV. Based on the results presented, the chiller system can provide comfort even when the chilled water temperature setpoint is increased to 14 °C.

3.2 Modelling and validation

To analyse the energy consumption of the chiller system under different CWTS, the numerical model of the chiller system was built, and its accuracy was validated by comparison with the experimental data.

3.2.1 Chiller

The results of the modelled chiller are summarized in Figs. 5a, b and 6 for 10 °C, 12.5 °C, and 14 °C CWTS, respectively. From the model validation results, the mean absolute error (MAE) for 10 °C, 12.5 °C, and 14 °C CWTS are 1.149 kWh, 1.041 kWh, and 0.497 kWh. All modelled chiller MAE results are reasonable with the chiller model results for 14 °C CWTS (0.497 kWh) being the least. The percentage of bias (PBIAS) which measures the average tendency of the simulated (results) to be larger or smaller than their observed counterparts (experimental results) was computed for the various CWTS. All PBIAS results were positive and, thus, indicate underestimation bias. The performance rating for modelled chiller PBIAS results is very good (5.513) for CWTS at 10 °C, good (10.898) for CWTS at 12.5 °C, and very good (0.907) for CWTS at 14 °C. The computed root mean square error (RMSE) results for the chiller at 10 °C, 12.5 °C, and 14 °C CWTS are 5.731, 4.637, and 2.189. RMSE-observations standard deviation ratio (RSR) results for modelled chiller are 0.268, 0.444, and 0.18 for CWTS at 10 °C, 12.5 °C, and 14 °C, respectively. The RSR performance rating results are very good for all the modelled chiller CWTS. By carefully examining the modelled chiller results, it is found that all chiller power consumed results for both the experimental and TRNSYS models show similar trends and the TRNSYS model is fairly accurate. However, the reason for disagreement between predicted and experimental results of power consumption in the late afternoon could result from the following: (1) the model

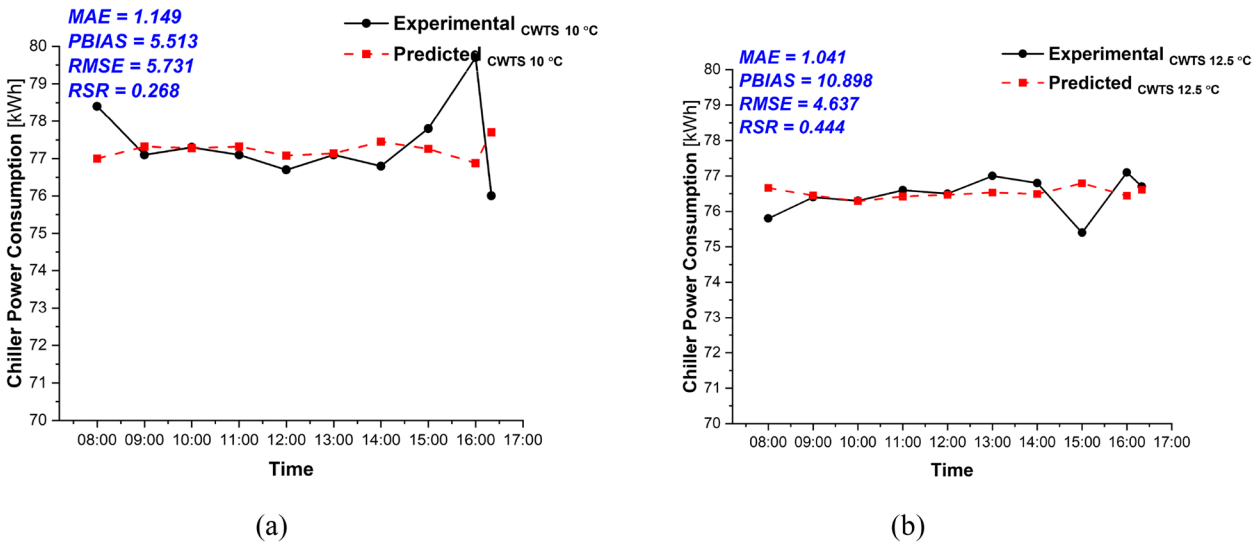

Fig. 5 Plot of total power consumed by chiller system at CWTS 10 °C (**a**) and 12.5 °C (**b**)

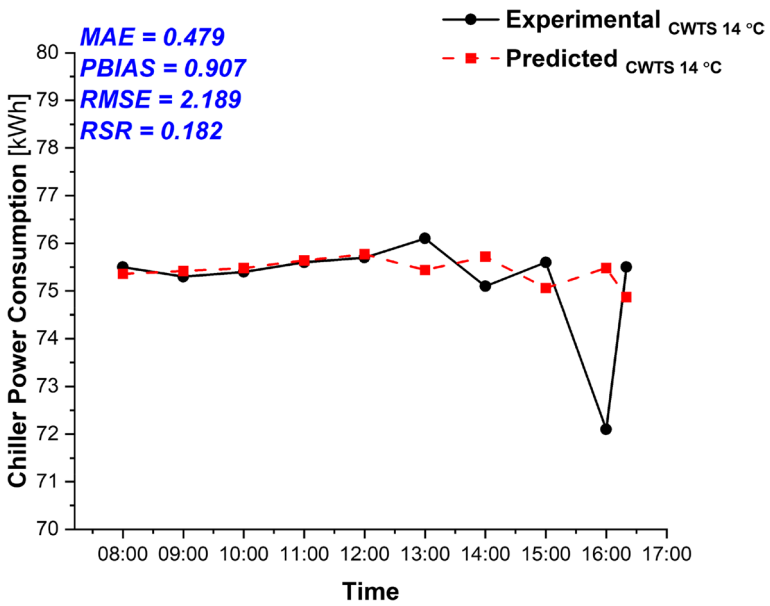

Fig. 6 Plot of total power consumed by chiller system at 14 °C

assumed a constant occupancy of six and behaviour patterns; however, it could be that there were variations in occupancy due to certain activities or real occupants have different habits at those hours of the day. (2) The weather data used in the modelling was the one for the whole Takoradi and may not match the actual weather conditions during that time of the experiment. (3) The model may not fully consider the thermal mass and inertia of the building, which can lead to differences in how quickly the space heats up or cools down in response to changes in outdoor conditions. These modelled chiller results have demonstrated better performance and thus TRNSYS can be used to effectively chiller results. Notwithstanding, this study is also limited by its consideration of only a hot humid climatic condition.

3.2.2 Fan coil unit

Figures 7a. b and 8 show the plot of total power consumed by fan coil unit at 10 °C, 12.5 °C, and 14 °C CWTS, respectively. The mean absolute error (MAE) values computed for the various CWTS (10 °C, 12.5 °C, and 14 °C) was 0.000 kWh for the modelled fan coil unit.

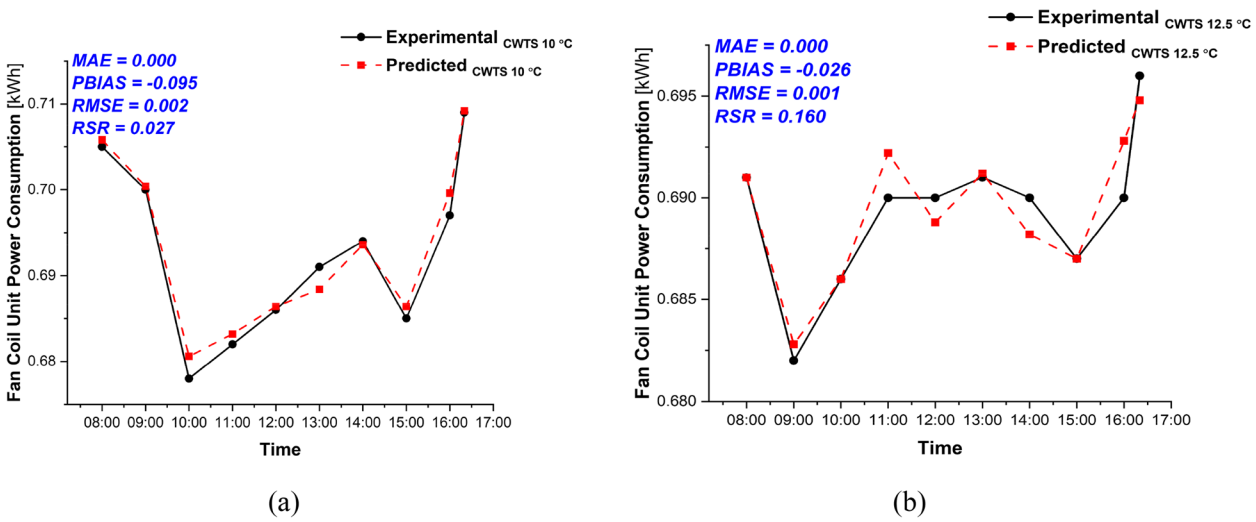

Fig. 7 Plot of total power consumed by fan coil unit at CWTS 10 °C (**a**) and 12.5 °C (**b**)

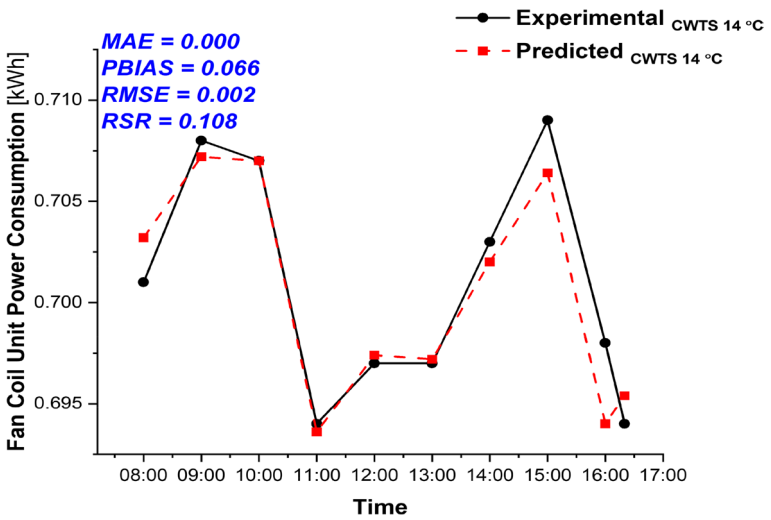

Fig. 8 Plot of total power consumed by fan coil unit at CWTS 14 °C

The calculated percentage of bias (PBIAS) values were −0.095, −0.026, and 0.066 for the 10 °C, 12.5 °C, and 14 °C CWTS, respectively. PBIAS results for 10 °C and 12.5 °C CWTS indicate overestimation bias, whereas PBIAS results for 14 °C CWTS show underestimation bias performance rating for modelled fan coil unit. PBIAS results are very good (PBIAS values for all CWTS were very good). The root mean square error (RMSE) results for the fan coil unit at 10 °C, 12.5 °C, and 14 °C CWTS are 0.002, 0.001, and 0.002, respectively. RMSE results for the fan coil unit show that both experimental and predicted (TRNSYS) fit well. RMSE-observations standard deviation ratio (RSR) results for modelled fan coil units are 0.027, 0.016, and 0.108 for CWTS at 10 °C, 12.5 °C, and 14 °C, respectively. All RSR performance rating results for the fan coil unit are very good. The results demonstrate that the fan coil unit TRNSYS model is fairly accurate and thus can be used to predict system performance. Overall, the model validation results are interesting and help to justify the popular use of TRNSYS as a building energy simulation (BES) software.

3.2.3 Pump

Plots of pump total power consumed showing experimental and predicted (TRNSYS) results are summarized in Figs. 9a, b and 10 for the various CWTS (10 °C, 12.5 °C, and 14 °C), respectively. Mean absolute error (MAE) results for the pump are 0.001 kWh, 0.001 kWh, and 0.002 kWh for 10 °C, 12.5 °C, and 14 °C CWTS, respectively. The computed PBIAS results are −0.010,

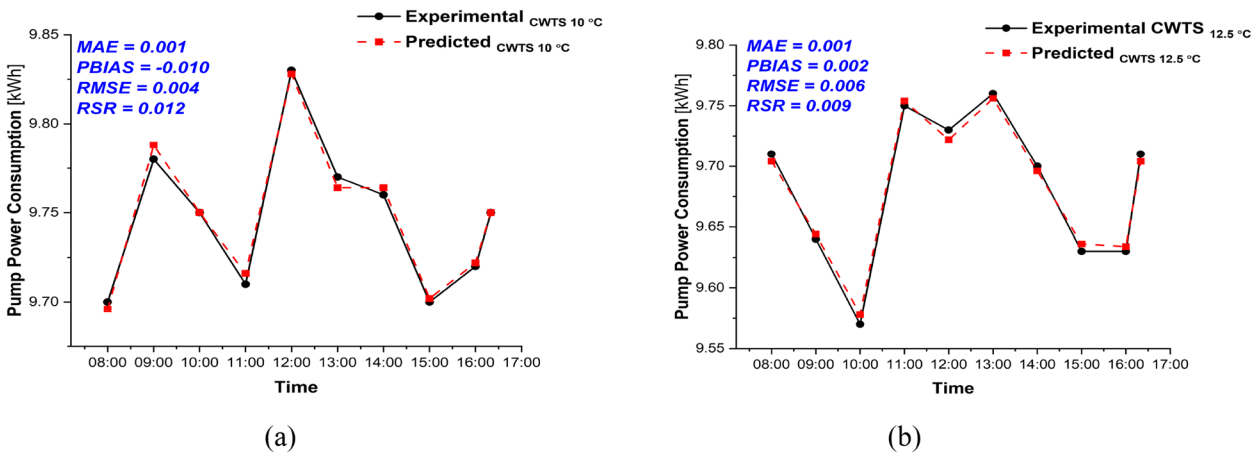

Fig. 9 Plot of total power consumed by the pump at CWTS 10 °C (**a**) and 12.5 °C (**b**)

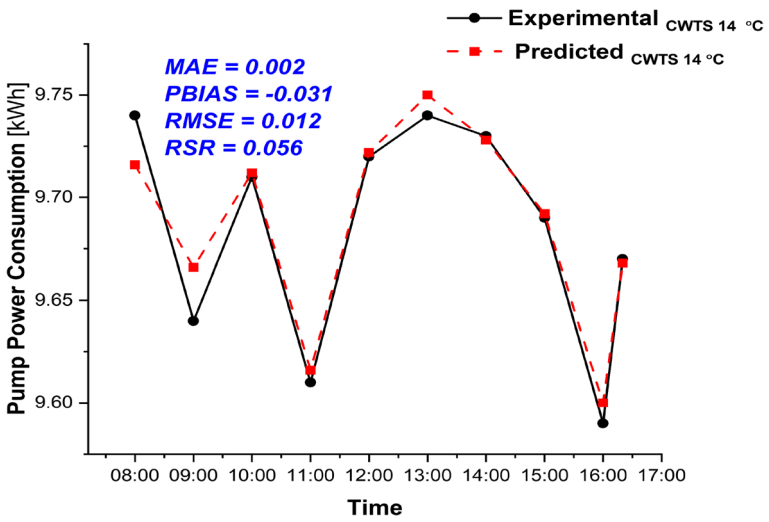

Fig. 10 Plot of total power consumed by the pump at CWTS 14 °C

0.002, and −0.031 for 10 °C, 12.5 °C, and 14 °C CWTS, respectively. PBIAS performance rating for the pump is very good. However, PBIAS results for 10 °C and 14 °C CWTS show overestimation bias, whereas PBIAS results for 12.5 °C CWTS indicate underestimation bias. Root mean square error (RMSE) results for the pump at 10 °C, 12.5 °C, and 14 °C CWTS are 0.004, 0.006, and 0.012, respectively. The low RMSE values indicate a close fit between experimental and predicted (TRNSYS) results. Pump RMSE-observations standard deviation ratio (RSR) results for 10 °C, 12.5 °C, and 14 °C CWTS are 0.012, 0.009, and 0.056. RSR performance rating results are very good for all the CWTS. The present results demonstrate better performance and can be used as a basis for pump system model development.

3.3 Prediction of chiller system performance beyond chilled water setpoint range

3.3.1 Chiller

The chiller accounts for the largest portion of total cooling energy consumption [44]. Therefore, reducing the energy consumption of the chiller is a key point to reduce

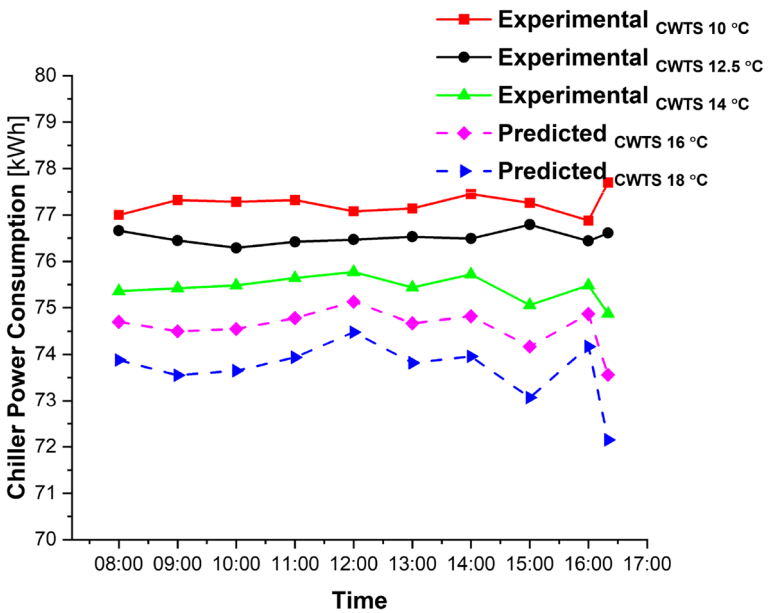

Fig. 11 Experimental and Predicted total power consumed by chiller

the overall cooling energy. Predictions were performed to compare the energy consumption of the chiller beyond the CWTS with the experimental data at different CWTS (10 °C, 12.5 °C, and 14 °C). Figure 11 shows the results of total energy consumed by the chiller at 10 °C, 12.5 °C, and 14 °C from the experiment and 16 °C, and 18 °C from the TRNSYS model predictions. Figure 12 shows the indoor thermal conditions at CWTS 18 °C. It can be seen from the results that the maximum and minimum energy consumed daily by the chiller was at 10 °C (77.4 kWh) and 18 °C (73.7 kWh) CWTS. Compared to the 10 °C CWTS, the chiller showed a low energy savings of 3% (at CWTS 14 °C), while it showed an energy savings of 5% (at CWTS of 18 °C). It can also be seen from the prediction that the higher the CWTS setpoint, the lower the energy consumed. This may result from the rise in the temperature and humidity caused by the increase in the CWTS and may require less energy to condition it. This is because when the temperature and humidity difference between indoor and ambient is slight, the workload of the HVAC system, including the cooling and dehumidifier system is less. Therefore, the CWTS could be set to a higher value for lower energy consumption and cost. However, raising the chilled water temperature may raise the air temperature, which will cause the fans to operate at higher power. Also, the increase in air temperature and humidity causes PPD to increase as evident in Fig. 4. Thus at 18 °C, the indoor thermal conditions do not fall in the comfort region as shown in Fig. 12 though a significant amount of energy would be saved. This result confirms the findings of Li et al. [45] that the exergy efficiency of the cooling terminal decreases by raising the chilled water temperature from 2 to 5 °C in Shanghai.

3.3.2 Pump and fan coil unit

The pump in the chiller system transports chilled water from the chiller to the fan coil unit. Figure 13a shows both experimental and predicted energy consumption results for the pump. The pump consumes daily average energy of 9.75, 9.68, and 9.63 kWh at 10 °C, 14 °C, and 18 °C CWTS, respectively. The results indicate that the amount of chilled water that must be pumped for a given cooling load is dependent on the CWTS.

Figure 13b shows the results of the energy consumed by the fan coil unit. The fan coil unit constitutes a fan and an assembly of coils that function primarily as a heat exchanger. The maximum energy consumed by the fan coil unit is relatively small (0.74 kWh) as compared to that of the chiller (79.72 kWh). The mean minimum and maximum energy consumed by the fan coil unit was 0.67 kWh at 10 °C CWTS (experimental) and 0.74 kWh at 18 °C CWTS (TRNSYS simulation). The results show that 18 °C CWTS recorded the highest energy consumption, unlike the chiller and pump which recorded lower energy consumption at higher CWTS. The high energy consumption at high CWTS could result from the fact that increasing the chilled water temperature increases the air temperature, which forces the fans to run at higher power. Thus, the specific fan power of the fan coil must be reduced to reduce the overall system energy

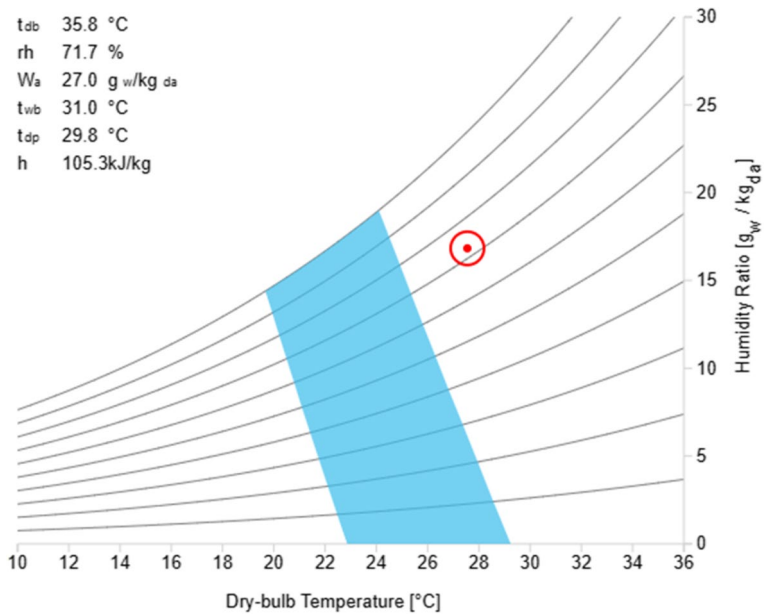

Fig. 12 Indoor thermal conditions at CWTS 18 °C

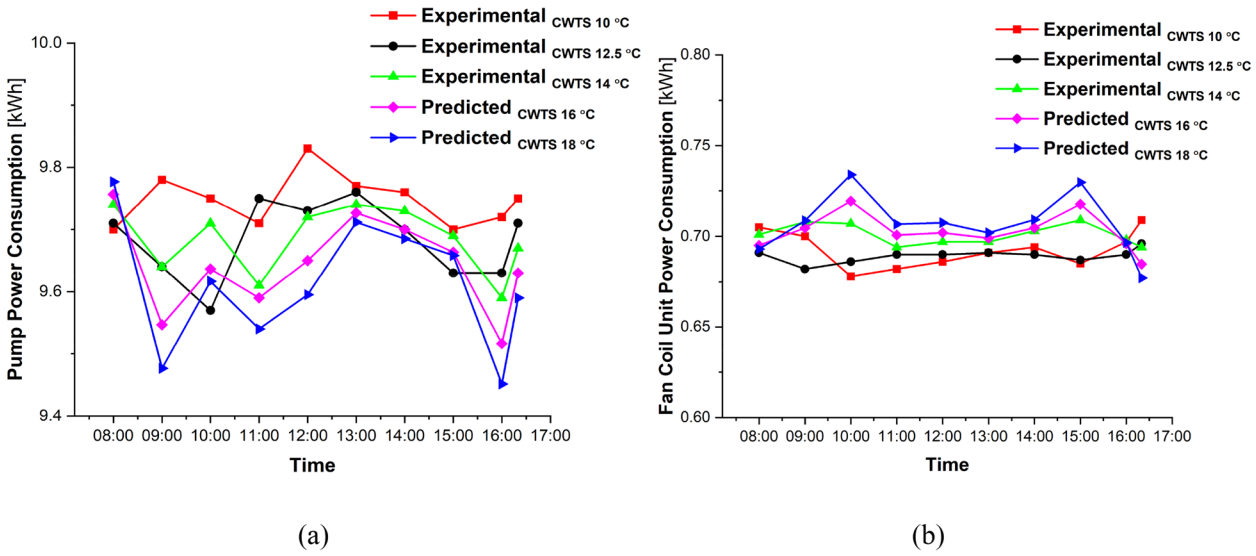

Fig. 13 Plot of power consumed by pump (**a**) and fan coil (**b**) (experimental and predicted)

consumption. Comparing the energy consumed by the fan coil at 10 °C CWTS to 14 °C and 18 °C CWTS, there is a percentage increase of 1% in energy consumption daily as against 18 °C CWTS (5.5%). The results clearly show that the fan-coil system with chilled water at 14 °C offered comfort (Fig. 4) and reduced energy consumption. This is in line with the assertion made in a study by Suzuki et al. [18] that chilled water at a temperature of 14 °C is successfully been used in Japan for space air conditioning. Conversely, the high CWTS may result in a decrease in the ability of the fan coil to cool and remove humidity (as seen in Fig. 4). This condition may be explained by the small logarithmic mean temperature differential (LMTD) between the chilled water in the fan coil and the indoor air. Therefore, it is important to investigate how to improve the fan-coil design after increasing the CWTS to guarantee a suitable level of indoor comfort and energy efficiency.

3.4 Optimizing the fan coil system

As can be seen from the findings, increasing the CWTS causes the fan coil unit to use more power and could make it uneconomical. Hence, the easiest way to improve the fan coil unit might be to make practical changes to some features or design elements. To study the combined effects of two or more elements on the fan coil, the design of experiment (DOE) was thus selected as the tool. Using design of experiment (DOE), influential parameters were varied to study how the fan coil could be improved. The factorial design analysis of the study is covered in the sections that follow. It includes the effects of inside tube diameter, number of rows, and CWTS on air temperature, logarithmic mean temperature difference (LMTD), and heat transfer coefficient (HTC).

3.4.1 Effects of inside tube diameter, number of rows, and CWTS on air temperature

A Pareto chart of standardized effects is shown in Fig. 14. According to the Pareto chart, CWTS (C) has the highest statistically significant standardized effect value of 88.66. The second-in-line, number of rows (B), with a normalized effect of 28.66, likewise has a statistically significant effect on air temperature. The effects of CWTS and the number of rows (BC) attained a standardized effect of 23.83. Effects of tube diameter and number of rows (AB), tube diameter (A), and tube diameter and CWTS (AC) had insignificant standardized effects of 1.76, 1.0, and 0.38, respectively, insignificant as a result of not crossing the reference line (12.71). The factors and effects discussed above that have significant effects should be taken into account when designing a fan coil since they affect the air temperature.

Figure 15 displays the main effect plot of air temperature. It demonstrates how CWTS has a significant influence on the highest air temperature (24.4 °C) (at CWTS of 14 °C), whereas the number of rows and tube diameter attained maximum air temperatures of 24.1 °C (at the low number of rows of 3) and 23.9 °C at tube diameter 7 to 9 mm. It can be seen that higher air temperature was achieved at 14 °C CWTS with 3 rows and tube diameter of 7 to 9 mm. The results confirm the assertion by Bai et al. [37] that as CWTS rises, the capacity of a three-row fan coil decreases, which could not be sufficient for indoor comfort. Hence, adding more rows of fan

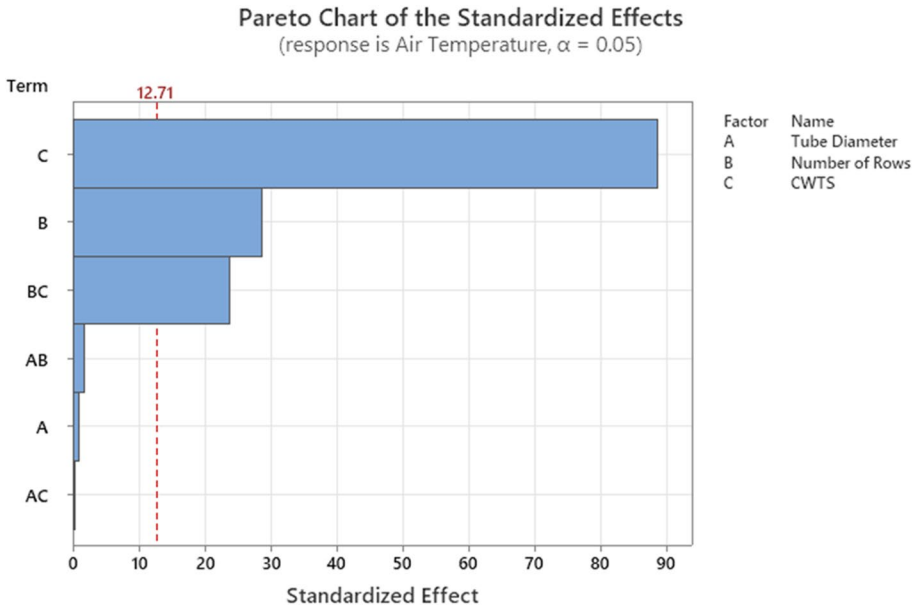

Fig. 14 Pareto chart of standardized effects (air temperature response, $\alpha = 0.05$)

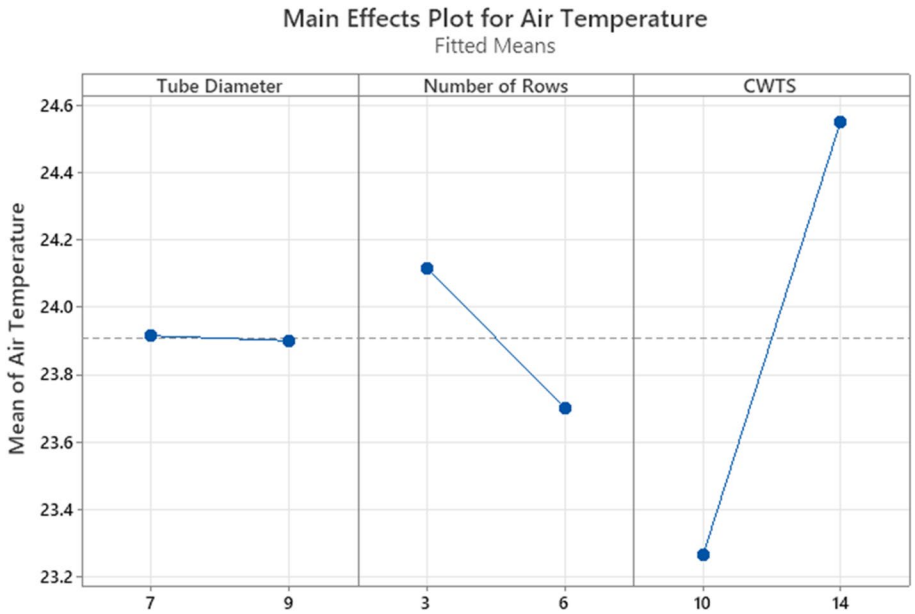

Fig. 15 Main effect plot for air temperature

coils would be a good solution to the capacity reduction issue. However, adding more tube rows may tend to grow the heat exchanger's size and footprint. This is because each additional row of tube requires additional space both in length and width dimensions which may require more space within an industrial facility or installation area. A larger heat exchanger may be required to accommodate the increased number of tubes. Also, the shape and configuration of the fan coil can be influenced by the number of tube rows. For example, a fan coil with a larger number of tube rows may have a longer, more rectangular shape compared to one with fewer rows which might be more compact and square. The configuration can also be influenced by the number of rows, with some configurations being more suitable for certain applications. The results showed that increasing the CWTS from 10 to 14

°C increases the air temperature. However, with a tube diameter from 7 to 9 mm and 6 rows of fan coils, optimal performance of the fan coil would be ensured. More tube rows result in a larger heat transfer surface area which allows for greater heat transfer between the fluids inside and outside of the tubes. As a result, heat exchangers with more rows can handle higher heat transfer rates. Therefore, improvement of the heat exchanger's thermal performance can be crucial in applications where maximizing heat transfer is a primary goal. The DOE results agreed with the experimental data well.

Figure 16 shows the interaction plot (plot of combined effects) of air temperature as influenced by tube diameter, number of rows, and CWTS. The plot of combined effects shows that the effects between tube diameter and number of rows were such that there was a rise in air temperature for a decrease in the number of rows (3) and tube diameter from 7 to 9 mm. The combined effect between tube diameter and CWTS showed that with increasing CWTS (10 to 14 °C) and tube diameter from 7 to 9 mm, the air temperature increases to 24.6 °C. Furthermore, the number of rows and the CWTS yields a high air temperature of 24.9 °C at 3 rows and 14 °C. However, increasing the number of tube rows in a heat exchanger generally increases the heat transfer surface area. This can improve the heat transfer rate, allowing the heat exchanger to handle higher heat loads. Hence, to attain the optimal functioning of the fan coil and enhance air temperature at elevated CWTS values, a synergistic impact resulting from a tube diameter increase (from 7 to 9 mm) coupled with six rows of tubes emerges as the most effective approach. It is observed that the combined effects plot (Fig. 16), the Pareto chart of standardized effects (Fig. 14), as well as main effects plot of temperature (Fig. 15), are all in good agreement.

Presented in Table 5 is the analysis of variance results for the effects of tube diameter, number of rows, and CWTS on air temperature. The *P*-value for all factors (number of rows and CWTS) except tube diameter is less than 0.05, which is statistically significant. It explains variation in the air temperature response. The regression results demonstrate a satisfactory fit of model variability for the air temperature. As a result, the regression model can be used to predict the fan coil air temperature.

3.4.2 Effects of inside tube diameter, number of rows, and CWTS on logarithmic mean temperature difference (LMTD)

An increase in LMTD improves heat transfer performance [46]. The Pareto chart of standardized effect presented in Fig. 17 shows the LMTD response. CWTS recorded the highest standardized effect of 28.14 which is beyond the reference line of 12.71. The rest (tube diameter, number of rows, and their effects had statistically insignificant effects on the LMTD of the fan coil since their standardized effects (−1.0, 1.0, −1.29) fall below the reference line (12.71).

The main effects plot for LMTD is presented in Fig. 18. The main effect plot shows that CWTS has the highest effect on the LMTD of the fan coil as compared to tube diameter and number of rows. It demonstrates that as the

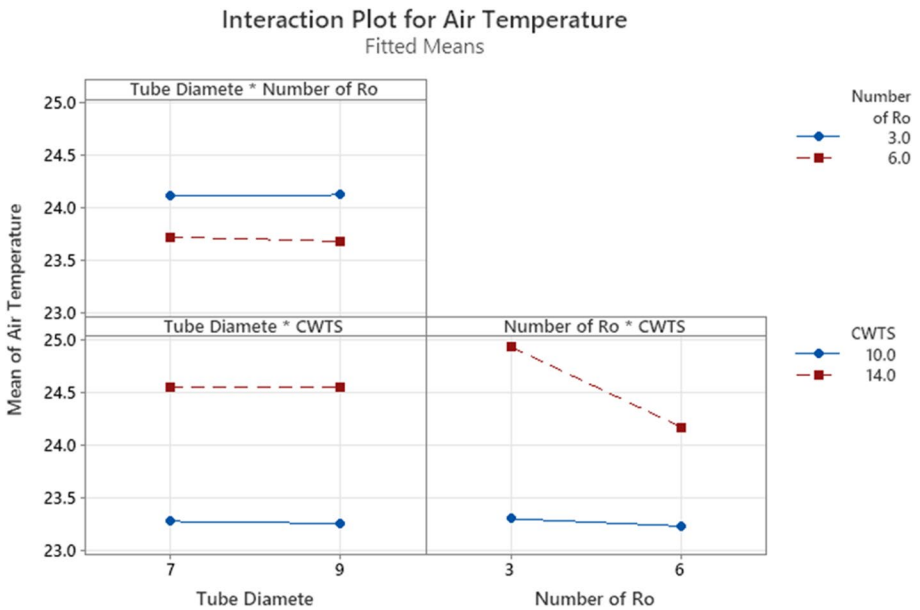

Fig 16 Interaction (combined effects) plot for air temperature

Table 5 The analysis of variance results for effects of inside tube diameter, number of rows, and CWTS on air temperature source

	DF[a]	Adj SS[b]	Adj MS[c]	*F*-value[d]	*P*-value[e]
Model	6	3.89082	0.64847	1542.14	0.019
Linear	3	3.65072	1.21691	2893.95	0.014
Tube diameter	1	0.00042	0.00042	1.00	0.500
Number of rows	1	0.34528	0.34528	821.12	0.022
CWTS	1	3.30502	3.30502	7859.74	0.007
2-way interactions	3	0.24010	0.08003	190.33	0.053
Tube diameter × Number of Rows	1	0.00130	0.00130	3.09	0.329
Tube Diameter × CWTS	1	0.00006	0.00006	0.14	0.769
Number of Rows × CWTS	1	0.23874	0.23874	567.75	0.027
Error	1	0.00042	0.00042		
Total	7	3.89124			

[a] Degrees of freedom

[b] Sum of squares

[c] Mean squares

[d] Ratio of variance of a source to variance of error

[e] Determines significance at 95% confidence level = $P < 0.05$

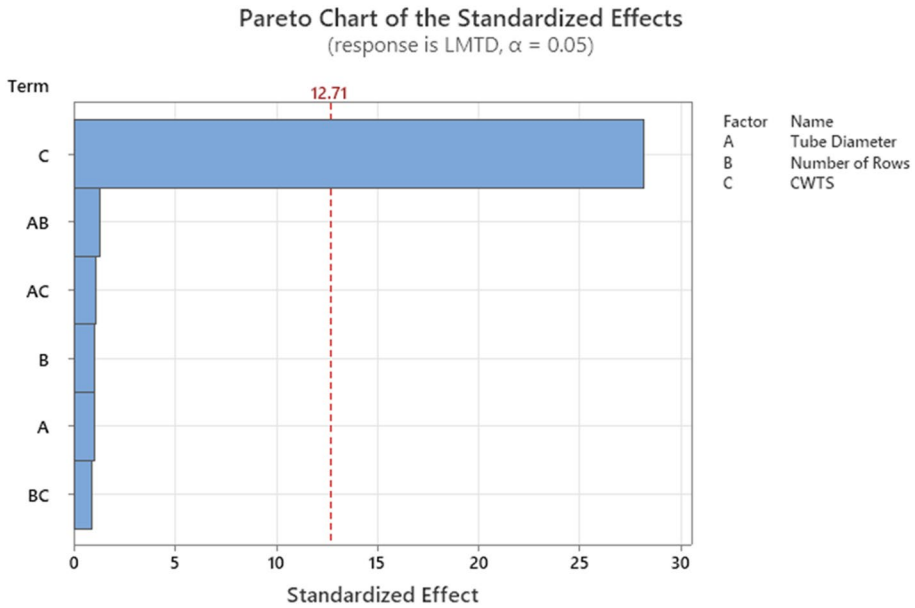

Fig 17 Pareto chart of standardized effects (LMTD, $\alpha = 0.05$)

CWTS increases the LMTD decreases, which may lead to poor heat transfer performance of the fan coil.

The results from the combined effect plots (Fig. 19) show that 10 °C CWTS with 3 rows, 10 °C CWTS with 7 mm tube diameter, and 3 rows with 9 mm tube diameter yield the highest mean LMTD and are therefore good factors for increased LMTD. The results confirm the assertion by Trane [46] that to increase the LMTD, the coils should be supplied with colder water. Conversely, the low chilled water temperature would increase the energy consumption of the chiller. Therefore, under the condition of an increased CWTS, the highest LMTD can be attained when the tube diameter is enlarged (from 7 to 9 mm) and the number of rows reduced (from 6 to 3). Subsequently, the number of tube rows can influence the pressure drop within the heat exchanger. More rows typically increase the resistance to fluid flow through the heat exchanger. This can lead to a higher pressure drop due to increased fluid friction as the fluid passes through a greater number of tubes. This can affect the overall

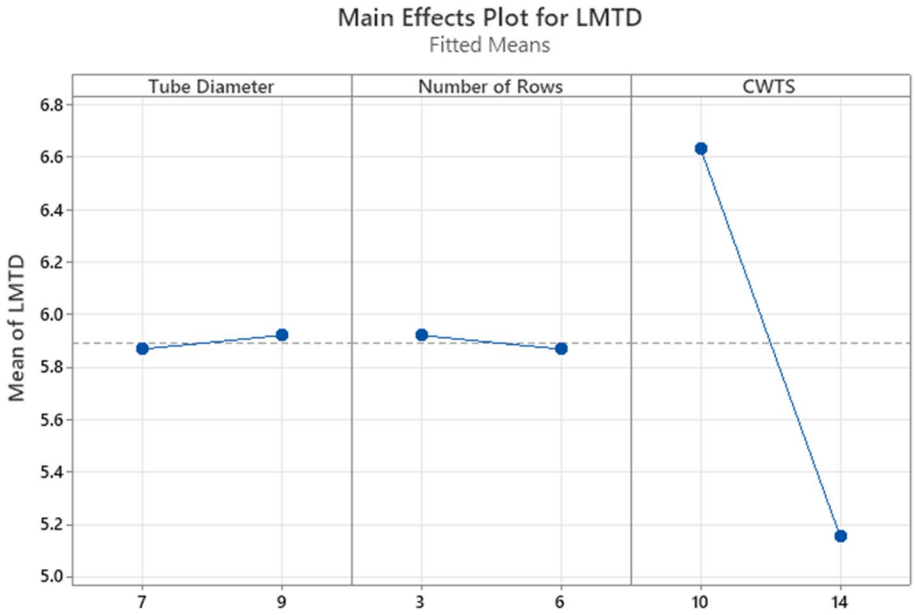

Fig. 18 Main effect plot for LMTD

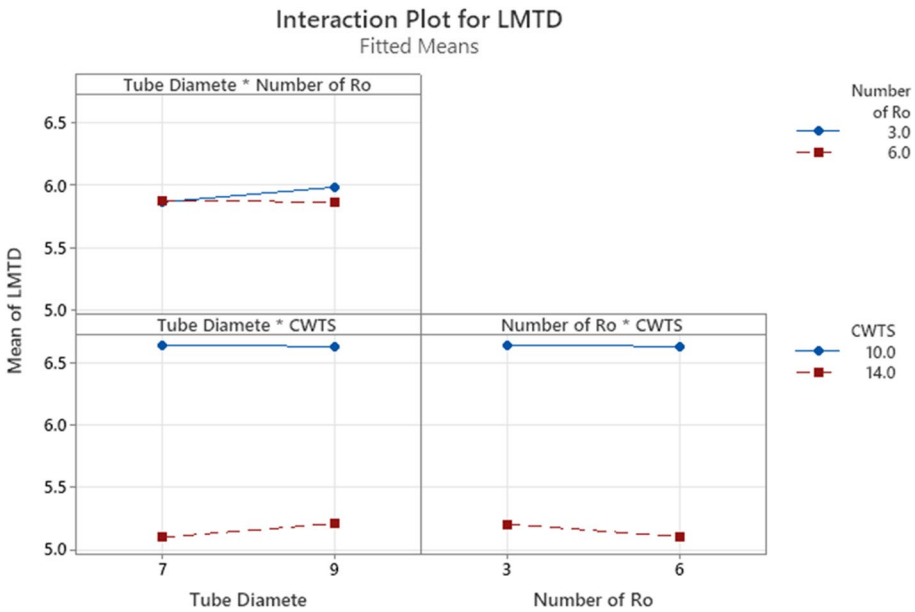

Fig. 19 Combined effects plot for LMTD

system design and the power required to pump the fluid through the exchanger.

Table 6 presents the analysis of variance results for the effects of inside tube diameter, number of rows, and CWTS on LMTD. Each term (inside tube diameter and number of rows) except CWTS is statistically insignificant since their *P*-value is more than 0.05. The regression results show a satisfactory fit of the model variability for the fan coil, and hence, the model can be used to predict the LMTD of the fan coil.

3.4.3 Effects of inside tube diameter, number of rows, and CWTS on heat transfer coefficient (HTC)

The rate of heat transfer increases with the heat transfer coefficient. Figure 20 is a Pareto chart of standardized effects. All the factors (tube diameter, number of

Table 6 The analysis of variance results for effects of inside tube diameter, number of rows, and CWTS on LMTD

Source	DF	Adj SS	Adj MS	*F*-value	*P*-value
Model	6	4.39727	0.73288	132.95	0.066
Linear	3	4.37704	1.45901	264.67	0.045
Tube diameter	1	0.00551	0.00551	1.00	0.500
Number of rows	1	0.00551	0.00551	1.00	0.500
CWTS	1	4.36601	4.36601	792.02	0.023
2-way interactions	3	0.02024	0.00675	1.22	0.567
Tube diameter × Number of Rows	1	0.00911	0.00911	1.65	0.421
Tube diameter × CWTS	1	0.00661	0.00661	1.20	0.471
Number of rows × CWTS	1	0.00451	0.00451	0.82	0.532
Error	1	0.00551	0.00551		
Total	7	4.40279			

rows, CWTS, and effects between them) had statistically insignificant effects on the HTC of the fan coil since their standardized effects (1.02, 9.48, −1.75, respectively) fall below the reference line (12.71).

Figure 21 shows the main effects of the heat transfer coefficient. The main effect plot shows that 3 rows of fan-coil had the largest heat transfer coefficient of 307.5 $W/m^2{\cdot}K$ as against 287.5 $W/m^2{\cdot}K$ of 6 rows. This result agrees with the findings of Pirompugd et al. [47], who showed that more rows have less impact on heat and mass transfer performance.

A tube diameter of 7 mm achieved the highest heat transfer coefficient (HTC) of 298 $W/m^2{\cdot}K$, surpassing that of the 9 mm diameter. This is in agreement with Nuntaphan et al. [48] whose research on crimped spiral coils in wet conditions indicated that smaller tube diameters resulted in a higher heat transfer coefficient. Moreover, the Chilled Water Temperature Setpoint (CWTS) of 14 °C exhibited the most substantial heat transfer coefficient (HTC) at 300 $W/m^2{\cdot}K$ compared to the 10 °C CWTS. This suggests that elevating the chilled water temperature results in an augmentation of the HTC. The results confirm Lee et al.'s [49] claim that the heat transfer coefficient increased as chilled water temperature increased.

Figure 22 shows the interaction plot (plot of combined effects) of the heat transfer coefficient as influenced by tube diameter, number of rows, and CWTS. The results show that 3 rows of fan-coil had the largest heat transfer coefficient when the tube diameter ranged from 7 to 9 mm. Also, the largest HTC was achieved with an increase in CWTS (14 °C) with a tube diameter of 7 mm. The effects between the number of rows and CWTS were such that the HTC was highest when CWTS increased from 10 to 14 °C, while the number of rows was up to 3. Therefore, under the condition of high CWTS, a combination of 7 mm tube diameter, 3-row fan coil, and 14 °C CWT will be the best candidates for high HTC for the fan coil. It can be seen that the combined effects plot (Fig. 22), Pareto chart of standardized effects (Fig. 20), as well as main effects plot of HTC (Fig. 21) are all in good agreement.

Table 7 presents the analysis of variance results for the effects of tube diameter, number of rows, and CWTS on

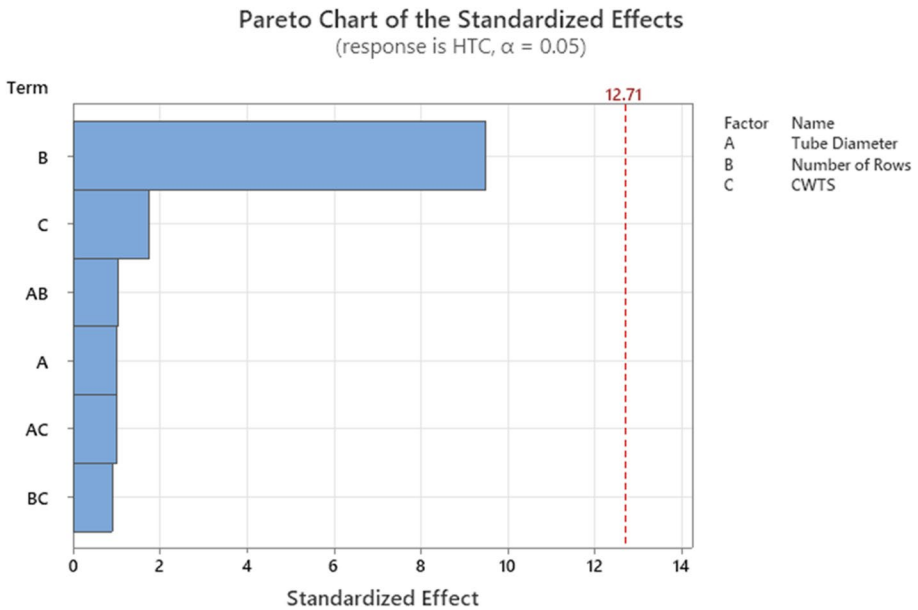

Fig. 20 Pareto chart of standardized effects heat transfer coefficient, $\alpha = 0.05$

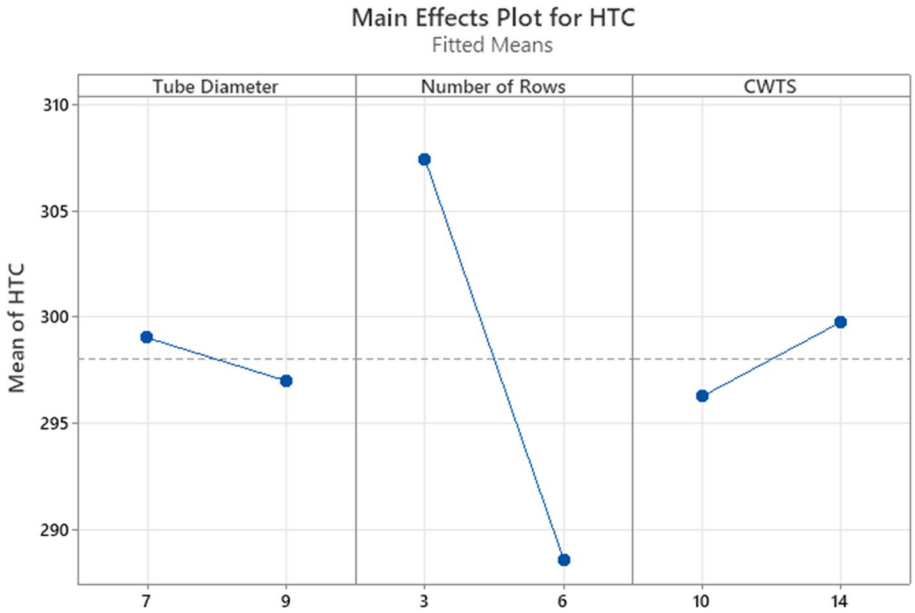

Fig. 21 Main effect plots for heat transfer coefficient

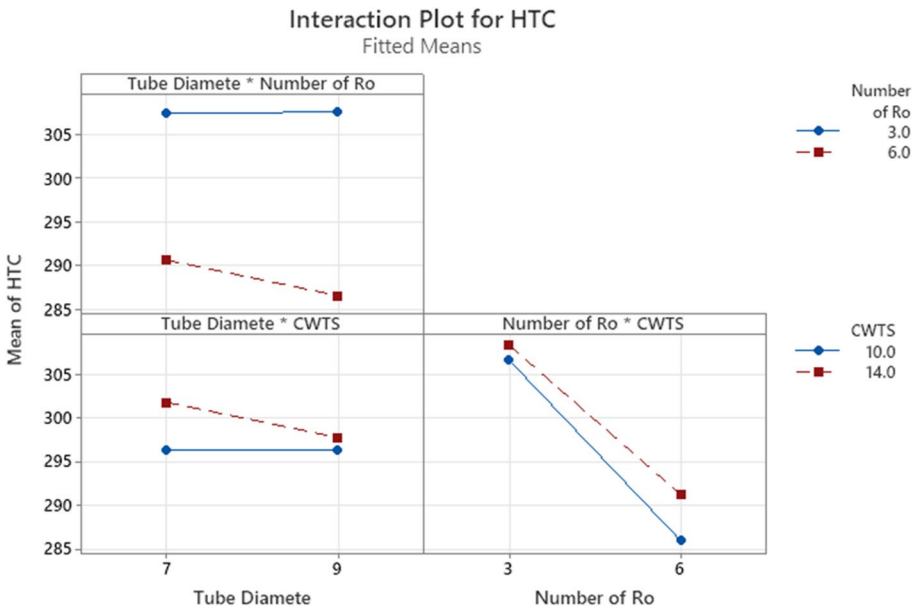

Fig. 22 Interaction plot (combined effects) of the heat transfer coefficient

the heat transfer coefficient. The *P*-value for each term (tube diameter, number of rows, and CWTS) is more than 0.05 which is statistically insignificant; however, the regression results show a satisfactory fit of the model variability for the fan coil heat transfer coefficient, and hence, the model can be used to predict the fan coil heat transfer coefficient.

4 Conclusion

This study proficiently examined the performance of the water-cooled chiller-fan coil system through a combination of modelling (utilizing TRNSYS and ASHRAE thermal comfort tool) and the implementation of a design of experiment (DOE) approach. The following are the key findings:

Table 7 The analysis of variance results for effects of inside tube diameter, number of rows, and CWTS on heat transfer coefficient

Source	DF	Adj SS	Adj MS	*F*-value	*P*-value
Model	6	766.503	127.750	16.13	0.188
Linear	3	743.891	247.964	31.31	0.130
Tube diameter	1	8.201	8.201	1.04	0.494
Number of rows	1	711.399	711.399	89.82	0.067
CWTS	1	24.290	24.290	3.07	0.330
2-way interactions	3	22.612	7.537	0.95	0.619
Tube diameter × number of rows	1	8.323	8.323	1.05	0.492
Tube diameter × CWTS	1	7.880	7.880	0.99	0.501
Number of rows × CWTS	1	6.408	6.408	0.81	0.534
Error	1	7.920	7.920		
Total	7	774.423			

1. The energy consumption attributed to the operation of the chiller system demonstrated that CWTS of 14 °C resulted in a slightly improved operation performance (3%) compared with CWTS of 10 °C. However, when the energy consumption at 18 °C was considered, it was determined that the continuous increment in the CWTS led to a further reduction (5%) in energy consumption. Resetting the CWTS from 10 to 14 °C causes an increase in the PMV. Based on the results presented, thermal comfort was achieved while consuming less energy even when the chilled water temperature setpoint was increased to 14 °C. However, at 18 °C CWTS, the indoor thermal conditions did not fall in the comfort region though a significant amount of energy was saved.
2. Additionally, the heat and mass transfer performance and design optimization of the fan coil with high CWTS were studied through experiment and simulation. The effect of CWTS, tube diameter, and number of rows on air temperature, LMTD, and HTC of the fan coil were studied. The results show that a 3-row fan coil cannot ensure an acceptable indoor air temperature when CWTS increases (from 10 to 14 °C). Therefore, increasing the row number (from 3 to 6) and increasing the tube diameter from 7 to 9 mm of the fan coil is an effective way to improve its cooling capacity.
3. In total, 10 °C CWTS with 3 rows, 10 °C CWTS with 7mm tube diameter, and 3 rows with 9 mm tube diameter yield the highest mean LMTD. However, under the condition of an increased CWTS, the highest LMTD can be attained when the tube diameter is enlarged (from 7 to 9 mm) and the number of rows reduced (from 6 to 3).
4. Also, under the condition of increased CWTS (14 °C CWT), a combination of a 7 mm tube diameter and a 3-row fan coil will be the best candidates for high HTC for the fan coil. To ensure the optimal performance of the fan coil, the optimal parameters of the fan coil can be obtained by combining the best factors. The optimal parameters for the efficiency of the fan coil were 14 °C, 6, and 9 mm for CWTS, row number, and tube diameter. Fan coil systems may be expected to yield an energy consumption that is lower than the existing energy consumption.

5 Future scope

The study focussed on comparing two values for tube diameter and number of tube rows in analysing the performance using DOE; however, future studies may develop an experimental setup based on the results of the study and subsequently consider more various values for tube diameter and number of tube rows for optimizing the coil design and study their effects.

Acknowledgements
This work was funded by the University of Johannesburg; South Africa and we would like to express our appreciation for their financial support to complete this work.

Authors' contributions
All the authors have contributed to the conceptualization, investigation, data collection, and analysis of the study and have read and agreed to the published version of the final manuscript.

Availability of data and materials
Data can be made available on request to the authors of the article. The data are not publicly available.

Declarations

Competing interests
The authors declare that they have no competing interests.

Received: 23 August 2023 Accepted: 30 November 2023
Published online: 15 December 2023

References

1. Amasuomo, T. T., & Amasuomo, J. O. (2016). Perceived thermal discomfort and stress behaviours affecting students' learning in lecture theatres in the humid tropics. *Buildings, 6*(2), 1–17.
2. Zaki, S. A., Hagishima, A., Fukami, R., & Fadhilah, N. (2017). Development of a model for generating air-conditioner operation schedules in Malaysia. *Building and Environment, 122*, 354–362.
3. Amoabeng, K. O., Opoku, R., Boahen, S., & Obeng, G. Y. (2023). Analysis of indoor set-point temperature of split-type ACs on thermal comfort and energy savings for office buildings in hot-humid climates. *Energy and Built Environment, 4*(3), 368–376.
4. EPA. (2017). *Ghana's greenhouse gas inventory and technology gap analysis for the refrigeration & air-conditioning sector* (pp. 1–80). Green Cooling Initiative.
5. Frontczak, M., & Wargocki, P. (2011). Literature survey on how different factors influence human comfort in indoor environments. *Building and Environment, 46*(4), 922–937.

6. Arif, M., Katafygiotou, M., Mazroei, A., Kaushik, A., & Elsarrag, E. (2016). Impact of indoor environmental quality on occupant well-being and comfort: A review of the literature. *International Journal of Sustainable Built Environment, 5*(1), 1–1.
7. Wei, X., Xu, G., & Kusiak, A. (2014). Modeling and optimization of a chiller plant. *Energy, 14*(73), 898–907.
8. Pérez-Lombard, L., Ortiz, J., Coronel, J. F., & Maestre, I. R. (2011). A review of HVAC systems requirements in building energy regulations. *Energy and Buildings, 43*(2-3), 255–268.
9. Wolkoff, P. (2018). Indoor air humidity, air quality, and health–An overview. *International Journal of Hygiene and Environmental Health, 221*(3), 376–390.
10. Perez-Lombard, L., Ortiz, J., & Maestre, I. R. (2011). The map of energy flow in HVAC systems. *Applied Energy, 88*(12), 5020–5031.
11. Energy, U. (2012). *2011 Buildings energy data book*.
12. Zhou, Y. P., Wu, J. Y., Wang, R. Z., Shiochi, S., & Li, Y. M. (2008). Simulation and experimental validation of the variable-refrigerant-volume (VRV) air-conditioning system in EnergyPlus. *Energy and Buildings, 40*(6), 1041–1047.
13. Cui, P., Yang, H., Spitler, J. D., & Fang, Z. (1985). Simulation of a hybrid ground-coupled heat pump with domestic hot water heating systems using HVACSIM+. *Energy and Buildings, 40*(9), 1731–1736.
14. Winkelmann, F. C., & Selkowitz, S. (1985). Daylighting simulation in the DOE-2 building energy analysis program. *Energy and Buildings, 8*(4), 271–286.
15. Lu L., & Cai W.(2001). Application of genetic algorithms for optimal chiller selection in HVAC systems. In 13th Int. Conference on Process Control.
16. Chang, Y. C., Lin, F. A., & Lin, C. H. (2005). Optimal chiller sequencing by branch and bound method for saving energy. *Energy Conversion and Management, 46*(13-14), 2158–2172.
17. Kusiak, A., Li, M., & Zheng, H. (2010). Virtual models of indoor-air-quality sensors. *Applied Energy, 87*(6), 2087–2094.
18. Suzuki Y., Imazu M., Shinoda J., Furukawa R., Araki Y., Tanabe S.I., Fujino K., Hatori D., Hirasuga N., Kato S., & Sasahara S. (2019). Efficient operation of heat source using high-temperature chilled water in an advanced office building, In E3S Web of Conferences, 111, 03071. EPD Sciences.
19. Ha, J. W., Cho, S., Kim, H. Y., & Song, Y. H. (2020). Annual energy consumption cut-off with cooling system design parameter changes in large office buildings. *Energies, 13*(8), 2034.
20. De Santoli L., Garcia D.A., Groppi D., Bellia L., Palella B.I., Riccio G., Cuccurullo G., d'Ambrosio F.R., Stabile L., Dell'Isola M., & Ficco G. (2018). A general approach for retrofit of existing buildings towards NZEB: The windows retrofit effects on indoor air quality and the use of low-temperature district heating. In 2018 IEEE International Conference on Environment and Electrical Engineering and IEEE Industrial and Commercial Power Systems Europe (EEEIC/I&CPS Europe) 1-6. IEEE.
21. Manfren M., Nastasi B., Piana E., & Tronchin L. (2019). On the link between energy performance of building and thermal comfort: An example. In AIP Conference Proceedings. 2123(1). AIP Publishing.
22. Šujanová, P., Rychtáriková, M., Sotto, M. T., & Hyder, A. (2019). A healthy, energy-efficient, and comfortable indoor environment, a review. *Energies, 12*(8), 1414.
23. Mancini, F., Nardecchia, F., Groppi, D., Ruperto, F., & Romeo, C. (2020). Indoor environmental quality analysis for optimizing energy consumption varying air ventilation rates. *Sustainability, 12*(2), 482.
24. Karami, M., McMorrow, G. V., & Wang, L. (2018). Continuous monitoring of indoor environmental quality using an Arduino-based data acquisition system. *Journal of Building Engineering, 19*, 412–419.
25. Vilčeková, S., Apostoloski, I. Z., Mečiarová, Ľ., Krídlová, B. E., & Kiseľák, J. (2017). Investigation of indoor air quality in houses of Macedonia. *International Journal of Environmental Research and Public Health, 1*, 37.
26. Nash, J. E. (1970). River flow forecasting through conceptual models, I: A discussion of principles. *Journal of Hydrology, 10*, 398–409.
27. Hnat T.W., Srinivasan V., Lu J., Sookoor T.I., Dawson R., Stankovic J., & Whitehouse K. (2011). The hitchhiker's guide to successful residential sensing deployments. In Proceedings of the 9th ACM Conference on Embedded Networked Sensor Systems, 232–245.
28. International Organization for Standardization. (2005). *Ergonomics of the thermal environment—Analytical determination and interpretation of thermal comfort using calculation of the PMV and PPD indices and local thermal comfort criteria*. International Organization for Standardization.
29. Standard, A.S.H.R.A.E (2017). Thermal environmental conditions for human occupancy. ANSI/ASHRAE, 66.
30. Hong, S. H., Lee, J. M., Moon, J. W., & Lee, K. H. (2018). Thermal comfort, energy, and cost impacts of PMV control considering individual metabolic rate variations in residential building. *Energies., 11*(7), 1767.
31. Díaz-Torres, Y., Valdivia-Noda, Y., Monteagudo-Yanes, J. P., & Miranda-Torres, Y. (2017). Application of building energy simulation in the validating of operational strategies of HVAC systems on a tropical hotel. *Ingeniería Mecánica, 20*(1), 31–38.
32. Levy, G. (2018). *Mathematical Reference. Energy power risk: Derivatives, computation, and optimization* (pp. 291–295). Emerald Publishing Limited.
33. Golmohammadi, G., Prasher, S., Madani, A., & Rudra, R. (2014). Evaluating three hydrological distributed watershed models: MIKE-SHE, APEX, and SWAT. *Hydrology., 1*(1), 20–39.
34. Wei, J., Li, Z., Xue, W., Sun, L., Fan, T., Liu, L., Su, T., & Cribb, M. (2021). The ChinaHighPM10 dataset: Generation, validation, and spatiotemporal variations from 2015 to 2019 across China. *Environment International, 146*, 106290.
35. Gupta, H. V., Sorooshian, S., & Yapo, P. O. (1999). Status of automatic calibration for hydrologic models: Comparison with multilevel expert calibration. *Journal of Hydrologic Engineering, 4*(2), 135–143.
36. Karunasingha, D. S. K. (2022). Root mean square error or mean absolute error? Use their ratio as well. *Information Sciences, 585*, 609–629.
37. Bai, M., Wang, F., Liu, J., & Wang, Z. (2021). Experimental and numerical studies of heat and mass transfer performance and design optimization of Fan-coil with high supply chilled water temperature in air-conditioning system. *Sustainable Energy Technologies and Assessments, 45*, 101209.
38. Yin, P., & Sang, Y. (2020). Model-based sensitivity analysis of barometric pressure on cooling capacity measurement of hydronic room fan coil units. *Science and Technology for the Built Environment, 27*(3), 316–328.
39. Zoran, M. A., Savastru, R. S., Savastru, D. M., & Tautan, M. N. (2020). Assessing the relationship between surface levels of PM2.5 and PM10 particulate matter impact on COVID-19 in Milan, Italy. *Science of the Total Environment, 738*, 139825.
40. Brągoszewska, E., Biedroń, I., Kozielska, B., & Pastuszka, J. S. (2018). Microbiological indoor air quality in an office building in Gliwice, Poland: Analysis of the case study. *Air Quality, Atmosphere and Health, 11*, 729–740.
41. Koranteng, C. (2010). Energy performance of office buildings in Ghana. *Journal of Science and Technology (Ghana), 30*(2), 114–127.
42. Zuo, C., Luo, L., & Liu, W. (2021). Effects of increased humidity on physiological responses, thermal comfort, perceived air quality, and sick building syndrome symptoms at elevated indoor temperatures for subjects in a hot-humid climate. *Indoor Air, 31*(2), 524–540.
43. Koranteng, C., Nyame-Tawiah, D., & Quansah, E. (2011). A psychrometric analysis of thermal comfort in low-rise office buildings in Ghana. *Journal of Science and Technology (Ghana), 31*(1), 76–88.
44. Chen, Z., Chen, Y., & Yang, C. (2022). Impacts of large chilled water temperature difference on thermal comfort, equipment sizes, and energy saving potential. *Journal of Building. Engineering, 49*, 104069.
45. Li, Z., Zhang, D., Chen, X., & Li, C. (2020). A comparative study on energy saving and economic efficiency of different cooling terminals based on exergy analysis. *Journal of Building Engineering, 30*, 101224.
46. Kim, J. K., Lee, G. C., Zhu, F. X. X., & Smith, R. (2002). Cooling system design. *Heat Transfer Engineering, 23*(6), 49–61.
47. Pirompugd, W., Wongwises, S., & Wang, C. C. (2006). Simultaneous heat and mass transfer characteristics for wavy fin-and-tube heat exchangers under dehumidifying conditions. *International Journal of Heat and Mass Transfer, 49*(1-2), 132–143.
48. Nuntaphan, A., Kiatsiriroat, T., & Wang, C. C. (2005). Heat transfer and friction characteristics of crimped spiral finned heat exchangers with dehumidification. *Applied Thermal Engineering, 25*(2-3), 327–340.
49. Lee, H., Hwang, Y., Radermacher, R., & Chun, H. H. (2013). Thermal and hydraulic performance of sinusoidal corrugated plate heat exchanger for a low-temperature lift heat pump. *International Journal of Refrigeration, 36*(3), 689–700.

Publisher's Note